Activation of Vibrational Stabilization in Insect-Like Flapping Systems

Ali Judi, Afshin Banazadeh*, and Amirali Asghari

Department of Aerospace Engineering, Sharif University of Technology, Tehran, Iran
Email: omoorsite92@gmail.com (A.J.); banazadeh@sharif.edu (A.B.); asghari936936@gmail.com (A.A.)
*Corresponding author
Manuscript received May 25, 2024; revised July 3, 2024; accepted September 1, 2024; published November 17, 2024

***Abstract*—Insect-like flapping wings, known for their complex multi-bodied structure and aerodynamically cyclic behavior, represent intricate aerial systems. Despite extensive engineering research over decades, many aerodynamic and dynamic phenomena governing these creatures remain inadequately understood. Of particular interest is vibrational stabilization, a phenomenon that significantly contributes to the inherent stability of specific types of these vehicles, acting as an open-loop inertial stability system. This study thoroughly examines the presence and effects of vibrational stabilization on the stability of an inverted oscillating pendulum and a six-degree-of-freedom model of an insect-like flyer. By analytically confirming the existence of this phenomenon and considering factors such as wing inertia and non-averaged aerodynamic forces, an investigation into the design parameters and their impact on the dynamic stability of the insect-like system has been conducted using a nonlinear simulation model.**

***Keywords*—insect-like flapping wings, vibrational stabilization, dynamic stability, nonlinear simulation model**

I. Introduction

In recent years, there has been a growing interest in small robotic flapping-wing systems due to their wide-ranging applications in various fields. These systems are utilized for tasks such as smart agriculture, search-and-rescue and exploration [1, 2]. In comparison with other aerial robots, flapping-wing systems exhibit superior maneuverability and aerodynamic efficiency, making them suitable for navigating through confined spaces, avoiding obstacles, and ensuring sustained flight. Among the stability mechanisms inherent in these systems, vibrational stabilization stands out as a significant contributor, acting as an open-loop inertial stability system.

Vibrational stabilization involves utilizing high-frequency oscillatory inputs to stabilize the motion of a system. The periodic flapping motion of these systems raises the question of whether this oscillatory movement can contribute to their stability. Traditionally, it has been believed that insects exhibit unstable hovering behavior due to their low torsional stiffness. However, recent publications and research in insect flight physics have provided evidence contradicting this notion [3].

The analysis of Flapping systems usually relies on two fundamental assumptions: neglecting the effects of wing inertia and averaging the flapping motion dynamics which serves as a standard technique for controller design in periodic systems. The first assumption is justifiable since the weight of the wing is typically less than 5% compared to the total weight. However, the main challenge lies in the second assumption, which presumes that the robot's response is based on the average of the periodic aerodynamic forces. This assumption eliminates certain aspects of the flapping systems' dynamic behavior. This issue was addressed by Taha [4, 5] by combining differential geometric control and averaging in a precise manner. In these investigations, the existence of a coupling between the high-frequency flapping dynamics and the low-frequency body dynamics was demonstrated, resulting in vibrational stabilization. His research combined rigorous differential geometric control with averaging techniques, revealing a fascinating phenomenon: a strong interaction between the high-frequency flapping dynamics and the low-frequency body dynamics in hovering insects and bio-inspired aerial robots. This interaction, surprisingly, leads to the emergence of a non-conventional stabilization mechanism known as vibrational stabilization. This technique, which is beneficial for unstable equilibrium systems, achieves stabilization through the application of a periodic force with suitable amplitude and frequency.

To provide an example, the unstable equilibrium of an inverted pendulum can be stabilized by oscillating its axis vertically at a high frequency. However, when it comes to the governing equations of a Kapitza pendulum (an inverted pendulum with a vertically oscillating axis), the averaging method fails to demonstrate the stabilizing effect of axis oscillation [6, 7]. Conversely, appropriate averaging techniques effectively revealed the stabilizing stiffness induced by the forced oscillation [8].

Prior research has often attributed the inherent instability of hovering flight in insects and insect-like robots to their low torsional stiffness [9–11]. However, Taha *et al*. [4, 5, 12] have challenged this belief. In these researches, an induced vibrational stabilization mechanism operating within the dynamics of these robots was identified, which acts as torsional stiffness. Additionally, it was demonstrated that the effect of wing inertia causes negative torsional stiffness and reduces torsional damping. Further investigation through vibrational stabilization, Taha *et al*. [13] experimentally validated the stabilizing effect of oscillation. Hassan *et al*. [14] conducted an analytical research, demonstrating that a high-frequency periodic force applied to flapping-wing robots induces vibrational stabilization to the slow body dynamics.

In previous studies, there have been notable weaknesses in understanding and addressing the phenomenon of vibrational stabilization in flapping systems. Despite significant research efforts, the intricate dynamics of insect-like flyers, particularly concerning their stability mechanisms, have remained inadequately explored.

However, the present research aims to address these shortcomings by conducting precise investigation on

vibrational stabilization in insect-like flapping systems. First, the phenomenon of vibrational stabilization in the inverted pendulum system is initially investigated as a simpler system. Then, the natural oscillation of insect-like robots, which induces a similar stability to that of the inverted pendulum system, is thoroughly examined. The objectives and innovations of this study encompass a comprehensive understanding and exploration of vibrational stabilization through analytical proofs, modeling, and simulations, accounting for wing inertia and temporal non-averaging effects. Furthermore, sensitivity analysis with respect to flapping design parameters will be conducted in insect-like robots in order to achieve a deeper comprehension of this phenomenon.

II. Dynamic Modeling

In this section, dynamic equations for the single-degree-of-freedom and the two-degree-of-freedom inverted pendulum are outlined, leading to the development of a dynamic model for the flapping robot.

A. Inverted Pendulum

Referring to Fig. 1, by incorporating damping and a sinusoidal excitation function, dynamic equations of the inverted pendulum can be derived.

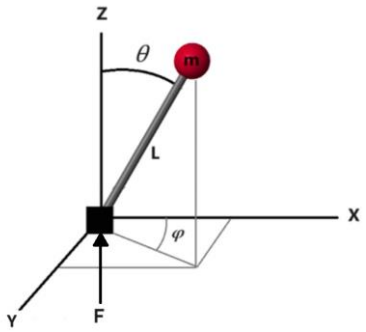

Fig. 1. Schematic of the inverted pendulum.

The Equations for both a one degree-of-freedom and two degree-of-freedom inverted pendulums are given by Eqs. (1)–(3):

$$\ddot{\theta} + \left(g \pm \frac{F}{m}\right) sin\,(\frac{\theta}{l}) + \frac{c\dot{\theta}}{ml^2} = 0 \tag{1}$$

$$\ddot{\theta} + \left(g \pm \frac{F}{m}\right) sin\,(\frac{\theta}{l}) - \frac{1}{2}\,\dot{\varphi}^2 \sin(2\theta) + \frac{c\dot{\theta}}{ml^2} = 0 \tag{2}$$

$$\ddot{\varphi}\ sin\ \theta + 2\dot{\theta}\dot{\varphi}\ cos\ \theta = 0 \tag{3}$$

Here, the excitation function F is given by:

$$F = Asin(2\pi ft) \tag{4}$$

where m, l, c, A and f are the pendulum mass, pendulum length, damping ratio and the amplitude and frequency of the excitation function.

B. Flapping Robot

To construct a dynamic model of the flapping robot, four frames are considered as shown in Fig. 2: earth-fixed inertial frame as **I**, body-attached frame as **B**, two stroke frames as $\mathbf{S_r}$ and $\mathbf{S_l}$ with the origins at the respective centers of mass of the hinges, H_r and H_l and finally, two wing frames as $\mathbf{W_r}$ and $\mathbf{W_l}$, each located at the respective centers of mass of the wings [15].

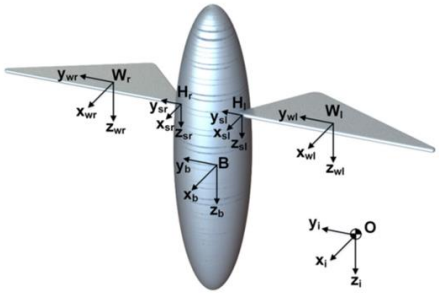

Fig. 2. Flapping robot frames [15].

The standard method for representing flapping motion involves Euler angles that define the wing's position in relation to the body, including φ for back and forth flapping, ϑ for plunging, and η for pitching angles as depicted in Fig. 3.

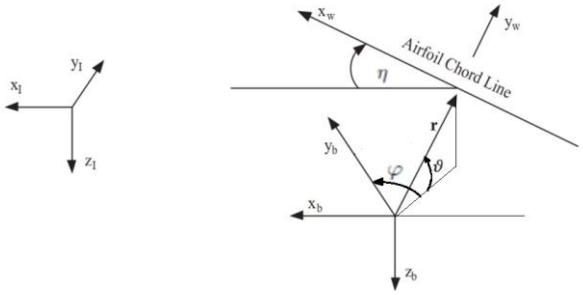

Fig. 3. Wing's angles ϑ, φ and η [16].

The principles of conservation of linear and angular momentum are applied to formulate the equations of motion with six degrees of freedom. Additionally, these equations are expressed with adjustments made to accommodate terms arising from rotating frames. Through the differentiation of rotational variables with respect to time, the classical equations of motion are redefined as follows:

$$m(D^B\mathbf{v} + \mathbf{\Omega}^{\mathrm{BI}}\mathbf{v}) = \sum \mathbf{F} \tag{5}$$

$$D^B\left(\boldsymbol{I}_{\mathrm{B}}^{\mathrm{B}}\boldsymbol{\omega}^{\mathrm{BI}}\right) + \mathbf{\Omega}^{\mathrm{BI}}\boldsymbol{I}_{\mathrm{B}}^{\mathrm{B}}\boldsymbol{\omega}^{\mathrm{BI}} = \sum \mathbf{M} \tag{6}$$

The sum of forces and moments on the right side of Eqs. (5) and (6) comprises two components: aerodynamic terms which are produced within the wing frames and necessitate transformation to the body frame and the term resulting from gravity acceleration in the inertial frame that must be transformed into the body frame. The required transformations matrices are defined in Eqs. (7)-(9) where s and c correspond to sin and cos. Also $[T]^{BI}$, $[T]^{WS}$ and $[T]^{SB}$ represent inertial to body, stroke to wing and body to stroke transformation matrices respectively.

$$[T]^{BI} = \begin{bmatrix} c\psi\ c\theta & s\psi\ c\theta & -s\theta \\ c\psi\ s\theta\ s\phi - s\psi\ c\phi & s\psi\ s\theta\ s\phi + c\psi\ c\phi & c\theta\ s\phi \\ c\psi\ s\theta\ c\phi + s\psi\ s\phi & s\psi\ s\theta\ c\phi - c\psi\ s\phi & c\theta\ c\phi \end{bmatrix} \tag{7}$$

$$[T]^{WS} = \begin{bmatrix} c\,\lambda\,c\,\phi & c\,\lambda\,s\,\phi & -s\,\lambda \\ -s\,\phi & c\,\phi & 0 \\ s\,\lambda\,c\,\phi & s\,\lambda\,s\,\phi & c\,\lambda \end{bmatrix} \quad (8)$$

$$[T]^{SB} = \begin{bmatrix} c\,\mu & 0 & -s\,\mu \\ 0 & 1 & 0 \\ s\,\mu & 0 & c\,\mu \end{bmatrix} \quad (9)$$

To explore aerodynamic forces, specific waveforms need to be established for wing translational and rotational motions. The prescribed functions denoted by $\phi(t)$ and $\lambda(t)$, aim to characterize wing movement:

$$\phi(t) = -A_\phi\, sin(2\pi f t + \phi_0) \quad (10)$$

$$\lambda(t) = A_\lambda sin\,(2\pi f t + \lambda_0) \quad (11)$$

A_ϕ and A_λ denote the maximum translational and rotational amplitudes, respectively, while f indicates the flapping frequency. Additionally, asymmetrical wing motion can be tuned using ϕ_0 and λ_0. Fig. 4 illustrates the proposed functions representing the wing's motion over a single period.

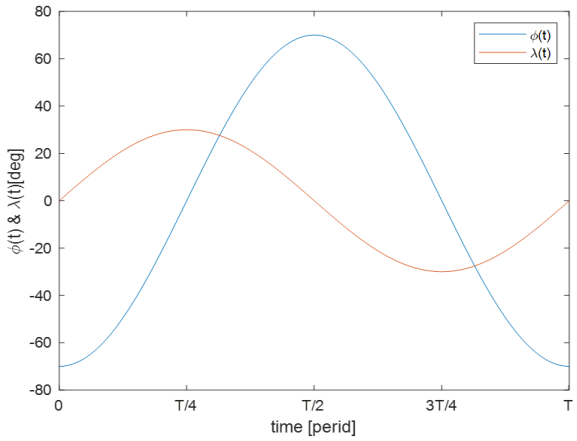

Fig. 4. Flapping and rotation functions.

Computational fluid dynamics (CFD) models are often used to study aerodynamics in flapping flight, but their complexity limits their application. Quasi-steady assumptions offer an alternative method, assuming aerodynamic forces are not dependent on wing motion history. Based on this method, two significant aerodynamic forces are considered in this research: delayed stall and rotational lift. Delayed stall, primarily responsible for lift production, occurs when the leading edge vortex remains attached to the wing surface at high angles of attack. Rotational lift, arising from the Magnus effect, occurs in two stages in flapping flight: during the upstroke and downstroke of the wing, and when the wing rapidly reverses its direction while having linear velocity. Delayed stall and the corresponding normal and tangential aerodynamic forces are considered based on the related coefficients as follow [17]:

$$F_n = \frac{1}{2}\,\rho v_{cp}^2 C_n S_w \quad (12)$$

$$F_t = \frac{1}{2}\,\rho v_{cp}^2 C_t S_w \quad (13)$$

where $C_n$and C_t are normal and tangential aerodynamic force coefficients and are computed as:

$$C_n = 3.4\, sin(\alpha) \quad (14)$$

$$C_t = \begin{cases} \cos^2(2\alpha), & |\alpha| < \frac{\pi}{4} \\ 0, & otherwise \end{cases} \quad (15)$$

$$\alpha = \lambda + \tan^{-1}\left(\frac{w_{cp}}{u_{cp}}\right) \quad (16)$$

The angle of attack (α) is defined as the angle formed between the mean aerodynamic chord and the wing's velocity vector.

Rotational lift has been modeled based on Eqs. (17) and (18) [18].

$$F_{rot} = \rho C_{rot} \dot{\alpha} \dot{\phi} \int_0^R r c^2(r) dr \quad (17)$$

$$C_{rot} = \pi(0.75 - \hat{x}_0) \quad (18)$$

Here $\hat{x}_0$ represents the normalized position of the pitch axis.

III. Simulation Results

A. Inverted Pendulum

The parameters required for simulating the inverted pendulum are detailed in Table 1.

Table 1. Parameters of the Inverted Pendulum

Parameter	Value	Parameter	Value
m	0.2 kg	c	0.0001 N-m/(deg/s)
r	0.2 m	A	0.05 m

In the initial investigation, a simulation of the inverted pendulum was conducted with the initial conditions of θ_0 = 10º and φ_0 = 15º. Fig. 5 displays the variations in θ and φ over time. It was observed that the two-degree-of-freedom pendulum remained stable when subjected to stimulation at the pivot joint which results from the vibration's stabilization effect.

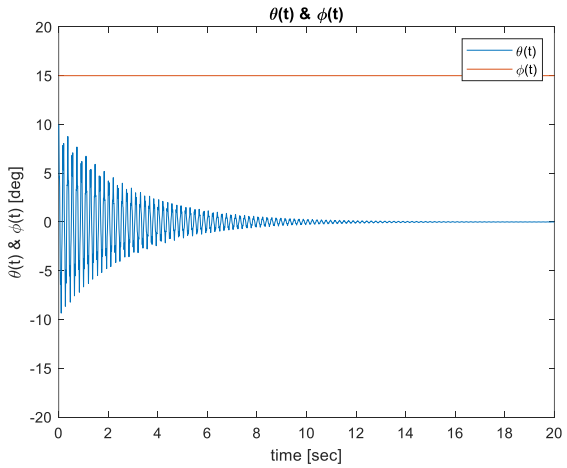

Fig. 5. Inverted pendulum response for θ_0 = 10º and φ_0 = 15º.

In the next investigation, the pendulum's response within a hypothetical scenario is examined as demonstrated in Fig. 6. Here, initial angles θ_0 and ϕ_0 are set to 10º and zero, respectively and at the tenth second, a force of 2 Newtons is also applied to the pendulum as a disturbance. Furthermore,

the excitation frequency is fixed at 30 Hz. It's evident that due to the appropriate oscillation, the system inherently maintains stability and effectively deflects any disturbances. It should be noted that during the scenario, angle ϕ remains zero.

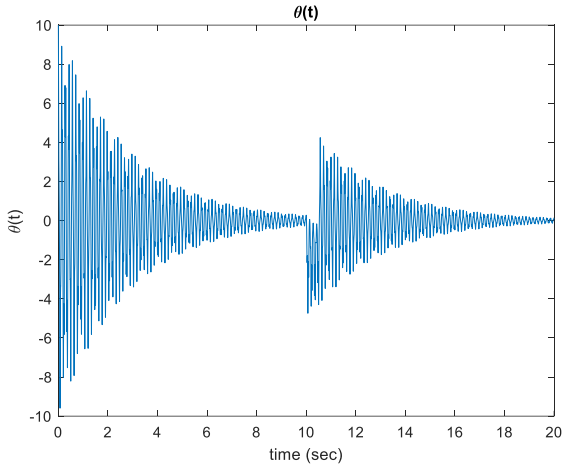

Fig. 6. Inverted pendulum inherent stability and disturbance rejection.

Applying sinusoidal force to the joint of an inverted pendulum through simulations in Matlab revealed that the inverted pendulum system becomes stable at a specific equilibrium point with a particular frequency and amplitude of excitation function. Its stability can be investigated using the Floquet theory. Floquet theory is a powerful method for analyzing the stability of time-varying dynamic systems subjected to periodic forces. It enables stability analysis for linear systems and finds various engineering applications.

As mentioned earlier, Eq. (1) represents the dynamic equation of a one degree-of-freedom inverted pendulum, with its joint excited by a sinusoidal external force F. To apply the Floquet theory to this equation, it first needs to be transformed into a system of linear differential equations with periodic coefficients. By linearizing the dynamic equations, one can obtain:

$$\dot{X} = A(t)X \tag{19}$$

$$X = \begin{bmatrix} x_1 \\ x_2 \end{bmatrix}, A(t) = \begin{bmatrix} 0 & 1 \\ \frac{-\left(g+\frac{F_0 sin(2\pi ft)}{m}\right)}{l} & -\frac{c}{ml^2} \end{bmatrix} \tag{20}$$

The matrix A(t) exhibits periodic behavior, implying the applicability of Floquet theory for stability analysis. According to Floquet theory, stability can be assessed by computing the monodromy matrix M, representing system evolution over a period, and evaluating its eigenvalues. If all eigenvalues of M have magnitudes less than one, the system is stable.

Considering Fig. 7, and applying the assumptions outlined in Table 1, the matrix M was computed across a frequency spectrum from 1 to 40 Hz. It was noted that the magnitude of the first eigenvalue of matrix M remains below 1 within the frequency range of 1 to 40 Hz. Conversely, the magnitude of the second eigenvalue of matrix M exceeds 1 up to frequency 6, satisfying the Floquet stability criterion and ensuring stability beyond the frequency of 7 Hz.

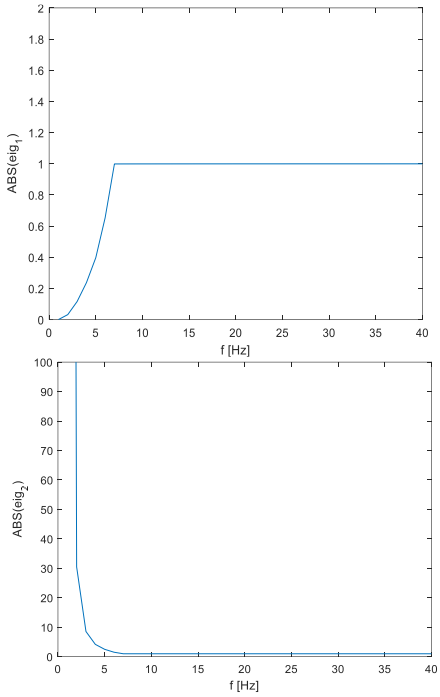

Fig. 7. The alterations in the magnitude of the first and second eigenvalues of matrix M with respect to variations in frequency.

To investigate better, it would be intriguing to derive the dimensionless parameters using the Buckingham π theorem for dimensional analysis. Utilizing the theorem, the dimensionless parameters are obtained as follows:

$$\left.\begin{array}{c} \Pi_1 = x m^a l^b f^c \\ L^0T^0M^0 = L^1M^aL^bT^{-c} \\ L: 0 = 1 + b \rightarrow b = -1 \\ T: 0 = -c \rightarrow c = 0 \\ M: 0 = a \rightarrow a = 0 \end{array}\right\} \Pi_1 = \frac{x}{l}$$

$$\left.\begin{array}{c} \Pi_2 = dex\, m^a l^b f^c \\ L^0T^0M^0 = L^1M^aL^bT^{-c} \\ L: 0 = 1 + b \rightarrow b = -1 \\ T: 0 = -c \rightarrow c = 0 \\ M: 0 = a \rightarrow a = 0 \end{array}\right\} \Pi_1 = \frac{dex}{l}$$

$$\left.\begin{array}{c} \Pi_3 = g m^a l^b f^c \\ L^0T^0M^0 = L^1T^{-2}M^aL^bT^{-c} \\ L: 0 = 1 + b \rightarrow b = -1 \\ T: 0 = -2 - c \rightarrow c = -2 \\ M: 0 = a \rightarrow a = 0 \end{array}\right\} \Pi_1 = \frac{g}{l\, f^2}$$

$$\Pi_1 = fcn(\Pi_2, \Pi_3) \tag{21}$$

$$\frac{x}{l} = fcn\left(\frac{dex}{l}, \frac{g}{lf^2}\right) \tag{22}$$

Where dex represents the amplitude of the excitation force (A in Eq. (4)), x denotes the initial distance of the pendulum from the origin of the coordinates along the X-axis. This value, in a sense, corresponds to the angle theta, given the length of the pendulum. In the previous step, according to Floquet theory, the minimum frequency for the stability of the system was found to be 7 Hz. Therefore, by substituting the parameters of the inverted pendulum, the dimensionless parameters are calculated as $\Pi_1 = 0.1736$, $\Pi_2 = 0.25$ and $\Pi_3 = 1.001$. By analyzing the provided values, it is observed

that reducing the excitation function's magnitude by half results in a corresponding minimum stability frequency of 10 Hz. This relationship is validated through simulations as demonstrated in Fig. 8.

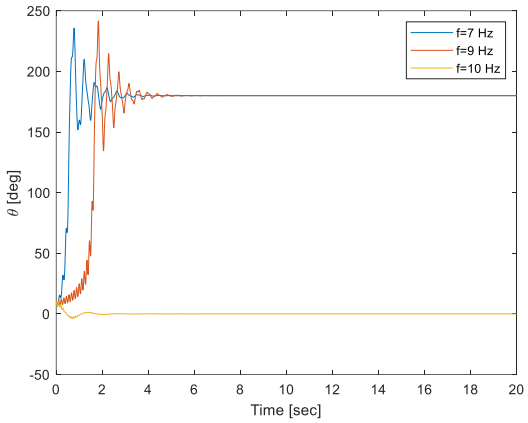

Fig. 8. System response for the excitation frequencies of 7, 9, and 10 Hz.

B. *Hummingbird Robot*

In this research, the flapping robot model represents a species of hummingbird as depicted in Figs. 9 and 10. The design parameters of the simulated hummingbird robot are presented in Table 2.

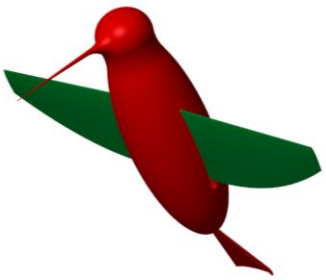

Fig. 9. 3D view of the flapping robot.

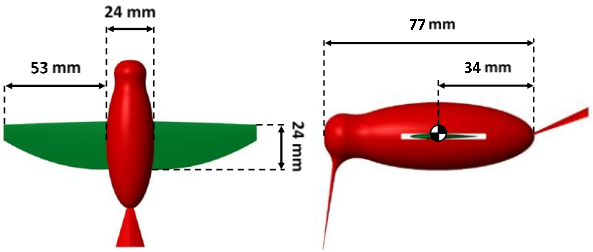

Fig. 10. Top and side view of the flapping robot.

Table 2. Parameters of the hummingbird robot

Parameter	Value	Parameter	Value
m_B	5.6 g	I_{XX_B}	472.2 g-mm^2
$m_{W_{L,R}}$	0.28 g	I_{YY_B}	2664.4 g-mm^2
l	77 mm	I_{ZZ_B}	2636.4 g-mm^2
b	130 mm	I_{XX_W}	176.2 g-mm^2
R	53 mm	I_{YY_W}	24.7 g-mm^2
$\hat{x}_0$	0.5	I_{ZZ_W}	200.4 g-mm^2
x_{cp}	25 mm	S_W	1003.2 mm^2

When applying the averaging method, incorporating the wing mass, inertia, and a flapping frequency of 30 Hz, the position of the robot in inertial coordinates, Euler angles, angular velocities and linear velocities in the body frame are depicted in Fig. 11. Taking into account the mass and inertia of the wings, it is observed that the linear velocity along X-axis, denoted by u, varies significantly. Changes in linear velocity u lead to changes in the moment applied to the robot about the pitch axis. In fact, it can be written as:

$$M_{V_x}V_x = (\overline{M_{V_x}} + \Delta M_{V_x})(\overline{V_x} + \Delta V_x) \tag{23}$$

The averaging method only considers the average contribution value $\overline{M_{V_x}V_x}$ and disregards oscillatory contributions. Considering other parameters and particularly the term $\Delta M_{V_x}\Delta V_x$, an analytical expression can be derived for the vibrationally induced stiffness k_θ as [19]:

$$k_\theta = \frac{g}{2T}\int_0^T \left[M_{V_x}(t)t - \int_0^t M_{V_x}(\tau)d\tau\right]dt \tag{24}$$

where M represents the derivative of stability, T denotes the periodicity, and g signifies the acceleration of gravity. This equation is derived from the second term of averaging and signifies the loss or omission of a value M_V when employing averaging techniques.

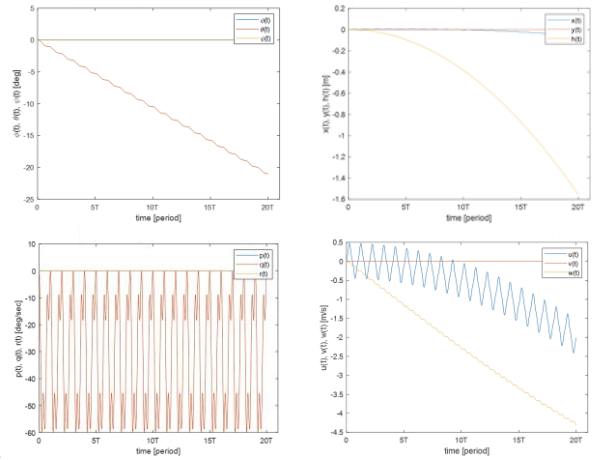

Fig. 11. The position of the robot in inertial coordinates, Euler angles, angular velocities and linear velocities using the averaging method.

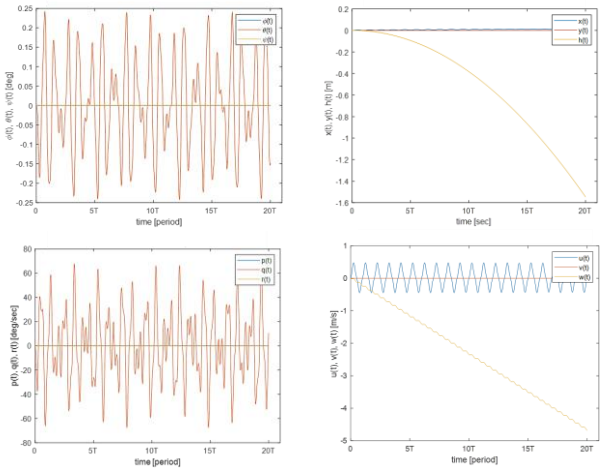

Fig. 12. The position of the robot in inertial coordinates, Euler angles, angular velocities and linear velocities considering the induced stiffness.

Assuming a constant λ for this robot, the value of k_θ is calculated as –0.0037886 N.m/deg. By incorporating the induced stiffness (k_θ) in addition to the wing mass, inertia,

and a flapping frequency of 30 Hz, the position of the robot in inertial coordinates, Euler angles, angular velocities and linear velocities in the body frame are presented in Fig. 12. As observed, the effect of stiffness k is quite significant in simulating the dynamics and has led to oscillatory stability.

Fig. 13 illustrates the inherent ability of the robot in rejecting disturbance for A_ϕ, A_λ, and f equal to 60º, 40º, and 30 Hz when imposing a disturbance (in the form of a force that has been applied to a point at the end of the bird's body) with an amplitude of 0.06 Newton at $t = 0.5$ s. It is evident that the pitch angle does not diverge, demonstrating an effective open-loop disturbance rejection.

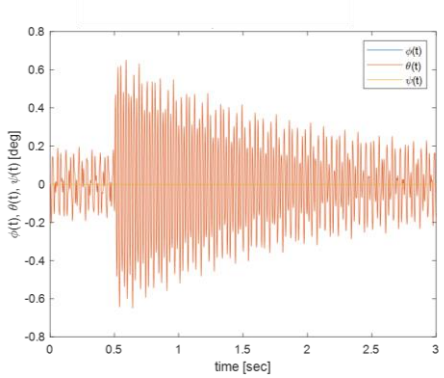

Fig. 13. System behavior in disturbance rejection at t=0.5 s.

Sensitivity analysis has been conducted to evaluate the effect of the pitch and flapping angle amplitudes on the robot response.

Figs. 14 and 15 depict the influence of variations in the wing pitch angle on the Euler angles and angular rates of the robot, considering vibrational stabilization. Furthermore, Figs. 16 and 17 depict the discussed sensitivity analysis concerning the wing flapping angle.

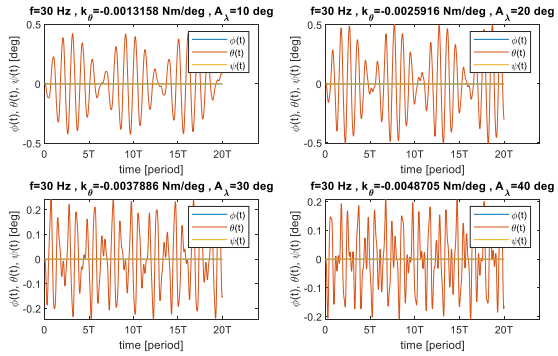

Fig. 14. Wing pitch angle-Euler angles sensitivity analysis.

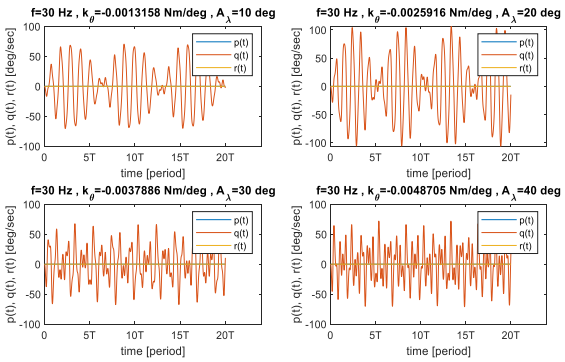

Fig. 15. Wing pitch angle-angular rates sensitivity analysis.

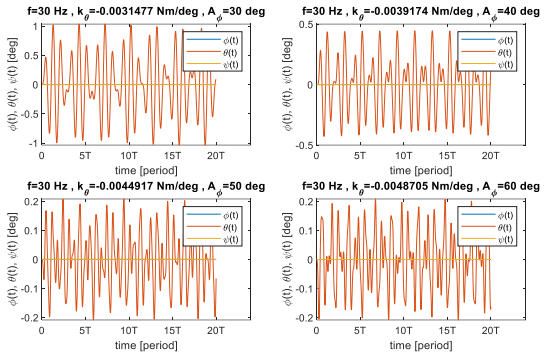

Fig. 16. Wing flapping angle-Euler angles sensitivity analysis.

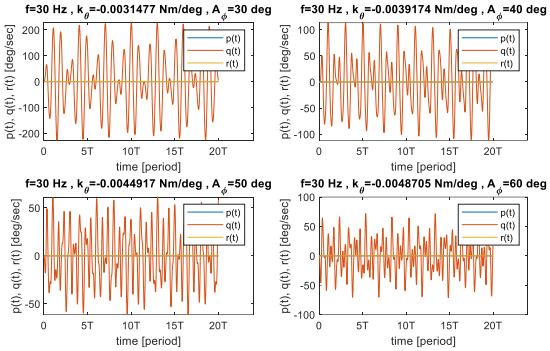

Fig. 17. Wing flapping angle-angular rates sensitivity analysis.

It is evident that when considering a broader range of pitch angles, there is a reduction in the amplitude of the pitch oscillations. The decrease can be attributed to the influence of the range of aerodynamic forces acting on the wing on M_{V_x} parameter. Consequently, since the wing's mass induces gravitational force similar to aerodynamic forces, there exists a direct correlation between wing mass and coefficient k_θ. Therefore, the influence of wing mass on coefficient k_θ can be approximated by the ratio of wing mass to the aerodynamic forces. In fact, altering the flapping angle amplitude leads to changes in coefficient k_θ (Eq. (25)).

$$k_\theta = k_{\theta_{Aero}} + Km_w k_{\theta_{Aero}} \tag{25}$$

It is noted that by increasing the flapping angle amplitude, the oscillations of the pitch angle decrease.

It is important to note that a key condition for applying the equations derived from the averaging theory is that the flapping frequency must be at least 30 times the natural frequency of the system. Hence, in the equation, the flapping frequency should exceed 30 Hz. As averaging is performed over one cycle of oscillation, the impact of frequency on the value of k_θ is considered to be very minimal.

IV. Conclusion

Vibrational stabilization is one of the most critical phenomena that had been overlooked in the stability analysis of flapping wings. Previous investigations indicated that flapping wings were unstable in the flutter phase, but contrary to this belief, it has been observed that they are stable. This study confirms the presence of this phenomenon in flapping wings and identifies that increasing the amplitude of the flapping and pitching angles enhances bird stability. Considering the stability of a two-degree-of-freedom inverted

pendulum under vibrational excitation at the pivot point, it was deduced that oscillation perpendicular to the unstable axis of the robot leads to the robot stability. Therefore, the flapping oscillations of wings will stabilize the pitch and yaw angles, though this study only considered the pitch stability. Extending this principle, the impact of this phenomenon on lateral stability can also be investigated. Moreover, constructing an oscillation-generating gadget can examine its effect on the stability of unconventional aerial robots, both analytically and experimentally. Exploring the optimal flapping conditions in real-world applications from a stability standpoint could present an intriguing avenue for future research.

CONFLICT OF INTEREST

The authors declare no conflict of interest.

AUTHOR CONTRIBUTIONS

The contributions of the authors to this study are significant and complementary. The first author played a key role in conducting simulations and meticulously analyzing the results obtained. Meanwhile, the second author was instrumental in conceptualizing the research topic and meticulously evaluating the outcomes. The third author took the lead in the writing process, crafting the manuscript with precision. All authors actively participated in the evaluation and revision stages of the paper, collectively ensuring its quality and coherence. All authors had approved the final version.

REFERENCES

[1] H. V. Phan and H. C. Park, "Insect-inspired, tailless, hover-capable flapping-wing robots: Recent progress, challenges, and future directions," *Prog. Aerosp. Sci.*, vol. 111, 100573, 2019.

[2] S. Abdullah, P. Appari, S. R. Patri, and S. Katkoori, "Smart agriculture using Flapping-Wing Micro Aerial Vehicles (FWMAVs)," in *Proc. IFIP International Internet of Things Conference*, 2021, pp. 32–47.

[3] H. E. Taha and M. Kiani, "A new vibrational control system in nature: Flapping flight," in *Proc. AIAA Scitech 2019 Forum*, 2019, 1417.

[4] H. E. Taha, S. Tahmasian, C. A. Woolsey, A. H. Nayfeh, and M. R. Hajj, "The need for higher-order averaging in the stability analysis of hovering mavs/insects," *Sel. Bioinspiration \& Biomimetics Highlights*, vol. 10, no. 1, 016002, 2015.

[5] H. E. Taha, A. H. Nayfeh, and M. R. Hajj, "Effect of the aerodynamic-induced parametric excitation on the longitudinal stability of hovering MAVs/insects," *Nonlinear Dyn.*, vol. 78, pp. 2399–2408, 2014.

[6] P. L. Kapitza, "Dynamical stability of a pendulum when its point of suspension vibrates, and pendulum with a vibrating suspension," *Collect. Pap. PL Kapitza*, vol. 2, pp. 714–737, 1965.

[7] P. L. Kapitza, "Pendulum with a vibrating suspension," *Usp. Fiz. Nauk*, vol. 44, no. 1, pp. 7–20, 1951.

[8] J. Baillieul, "Open-loop control using oscillatory inputs," *CRC Control Handb.*, 1996.

[9] M. Sun and Y. Xiong, "Dynamic flight stability of a hovering bumblebee," *J. Exp. Biol.*, vol. 208, no. 3, pp. 447–459, 2005.

[10] G. K. Taylor and A. L. R. Thomas, "Dynamic flight stability in the desert locust Schistocerca gregaria," *J. Exp. Biol.*, vol. 206, no. 16, pp. 2803–2829, 2003.

[11] G. K. Taylor and A. L. R. Thomas, "Animal flight dynamics II. Longitudinal stability in flapping flight," *J. Theor. Biol.*, vol. 214, no. 3, pp. 351–370, 2002.

[12] H. E. Taha, C. A. Woolsey, and M. R. Hajj, "Geometric control approach to longitudinal stability of flapping flight," *J. Guid. Control. Dyn.*, vol. 39, no. 2, pp. 214–226, 2016.

[13] H. Taha, M. Kiani, and J. Navarro, "Experimental demonstration of the vibrational stabilization phenomenon in bio-inspired flying robots," *IEEE Robot. Autom. Lett.*, vol. 3, no. 2, pp. 643–647, 2017.

[14] A. M. Hassan and H. E. Taha, "Differential-geometric-control formulation of flapping flight multi-body dynamics," *J. Nonlinear Sci.*, vol. 29, pp. 1379–1417, 2019.

[15] B. E. Wissa, K. O. Elshafei, and A. A. El-Badawy, "Lyapunov-based control and trajectory tracking of a 6-DOF flapping wing micro aerial vehicle," *Nonlinear Dyn.*, vol. 99, no. 4, pp. 2919–2938, 2020.

[16] H. E. Taha, "Mechanics of flapping flight: Analytical formulations of unsteady aerodynamics, kinematic optimization, flight dynamics, and control," Virginia Polytechnic Institute and State University, 2013.

[17] M. H. Dickinson, F.-O. Lehmann, and S. P. Sane, "Wing rotation and the aerodynamic basis of insect flight," *Science*, vol. 284, no. 5422, pp. 1954–1960, 1999.

[18] S. P. Sane and M. H. Dickinson, "The aerodynamic effects of wing rotation and a revised quasi-steady model of flapping flight," *J. Exp. Biol.*, vol. 205, no. 8, pp. 1087–1096, 2002.

[19] H. E. Taha, M. Kiani, T. L. Hedrick, and J. S. M. Greeter, "Vibrational control: A hidden stabilization mechanism in insect flight," *Sci. Robot.*, vol. 5, no. 46, eabb1502, 2020.